1 **The first Earthquake Early Warning System for the high-speed railway in Italy: enhancing rapidness**

2 **and operational efficiency during seismic events**

3 Simona Colombelli[1], Aldo Zollo[1], Francesco Carotenuto[1], Alessandro Caruso[1,2], Luca Elia[1], Gaetano

4 Festa[1], Sergio Gammaldi[1,3], Antonio Giovanni Iaccarino[1], Giovanni Iannaccone[1], Alberto Mauro[2],

5 Matteo Picozzi[1], Giulia Polimanti[2], Rosario Riccio[1,4], Stefania Tarantino[1,5], Francesco Cirillo[2],

6 Andrea Vecchi[2], Franco Iacobini[2].

7   1) Department of Physics, University of Naples Federico II, Italy

8   2) RFI – Rete Ferroviaria Italiana S.p.A., Italy

9   3) INGV – Catania, Italy

10   4) INGV – Osservatorio Vesuviano, Italy

11   5) INGV – L'Aquila, Italy

13 **Corresponding author:**

14 Simona Colombelli

15 Department of Physics, University of Naples Federico II

16 Complesso Universitario di Monte S.Angelo – Edificio 6, Via Cintia - 80126 Napoli

17 tel: +39 081 676346; e-mail: simona.colombelli@unina.it

19 **ABSTRACT**

20 Earthquake Early Warning (EEW) systems are modern, real-time seismic monitoring infrastructures

21 capable of identifying relevant earthquakes and providing warnings to population and infrastructures,

22 possibly before the arrival of the strongest shaking. Railway infrastructures represent a key target

23 application for EEW systems, due to their strategic role for public transportation of passengers and goods.

24 Here we describe the end-to-end system developed for the Naples-Rome high-speed railway that integrates

25 seismic monitoring, advanced signal processing, and railway-specific protocols to enhance the management

26 of railway operation in case of earthquakes in one of Italy's most seismically active regions.

27 The system utilizes a dedicated network of seismic stations equipped with accelerometers to detect ground

28 motion and predict Peak Ground Acceleration in real-time. A probabilistic decision-making module

29 evaluates seismic data and dynamically updates alerts as the P-wave propagates. Alerts are issued for the

30 Alerted Segment of the Railway, allowing operational restrictions like train deceleration or halting to

31 mitigate seismic impacts. The system minimizes unnecessary disruptions by targeting specific segments,

32 unlike traditional approaches that shut down entire lines.

33 The developed EEW system integrates train traffic control system, ensuring synchronized communication

34 between trains, signaling infrastructure, and control centers. This enables rapid activation of emergency

35 braking systems when required. Performance evaluations reveal high reliability, with rapid alerts issued

36 within 3–10 seconds and correct predictions in over 90% of cases.

37 Designed with scalability in mind, the system is exportable to other railway segments and adaptable to

38 diverse seismic networks. Its ability to generate real-time shake maps and refine alerts during seismic

39 events positions it as a global benchmark for integrating seismic management into high-speed rail

40 operations.

41

42 **Keywords**: Earthquake Early Warning; Seismic Risk Reduction; Earthquake Alerts; Real-time seismology

43

44

45

46 1. INTRODUCTION

47 Active faults are a serious threat for several regions in the world and many high-impact earthquakes of the

48 recent century have caused huge casualties, dramatic economic losses, and irreparable damage to historical

49 buildings as well as to critical, modern infrastructures (Firmi et al., 2020; Lakušić et al., 2020; W. Zhu et

50 al., 2020). An Earthquake Early Warning (EEW) system is a complex seismic monitoring infrastructure

51 that has the potential to provide warning to targets, potentially prior to strong ground shaking, mitigating

52 the impact of earthquakes in terms of fatalities, injuries and economic losses. This is possible through the

53 rapid detection of the early radiated signals from an ongoing earthquake and the fast issuing of information

54 on the expected ground shaking, either within the epicenter area or at far locations (Allen & Melgar, 2019;

55 Satriano et al., 2011).

56 During the last two decades, EEW systems have been widely developed and experimented in several high

57 seismic hazard countries around the world, such as Japan, USA, Mexico, Taiwan, China, Italy, Romania,

58 Switzerland, Turkey, Greece, and the Ibero-Maghrebian region (Allen & Melgar, 2019). At European scale,

59 Cremen et al. (2022) recently investigated the feasibility of EEW application and the potential effectiveness

60 of these systems across Europe and demonstrated that, some parts of Europe would benefit from real-time

61 alerts, with enough time to perform emergency actions (such as stopping traffic, stopping elevators,

62 shutting off gas supplies, among others).

63 In the context of EEW, railway infrastructures are of particular interest due to their strategic role for

64 private/public transportation of both passengers and goods (Minson et al., 2021; Nakamura & Saita, 2007;

65 Yamamoto & Tomori, 2013). High-speed railways are nowadays becoming the most popular and fast

66 transportation system, with trains achieving cruise velocities of several hundred km/h that demand

67 advanced systems for the railway signaling and remote/onboard control, in view of the application of

68 severe protection measurements for travelers. Despite the rapid progress in methodological/technological

69 developments in real-time seismic monitoring and source modelling, the interactions of EEW systems with

70 final end-user applications are still complex and under development. It requires that real-time

71 methodologies and technologies not only are validated and implemented at prototype level but also should

72 satisfy high levels of Technological Readiness (European Commission, 2014).

73 There are a few successful examples of application of EEW systems to normal or high-speed railway lines

74 in different active seismic regions of the world. Among them, the Urgent Earthquake Detection and Alarm

75 System (UrEDAS) (Nakamura, 1988; Nakamura & Saita, 2007) in Japan, the EEW system for the Bay

76 Area Rapid Transit (BART) train system in California (Strauss & Allen, 2016), the EEW system on the

77 high-speed railways in China (Tan et al., 2024; Yu et al., 2023; Zhang et al., 2024), and the EEW system

78 for Marmaray Tube Tunnel in Turkey (Clinton et al., 2016; Erdik et al., 2003).

79 This paper presents the first end-to-end application of EEW systems in Italy, fully targeted to a public

80 transportation infrastructure at national scale, managed by RFI (Rete Ferroviaria Italiana, the lead company

81 in the Infrastructure Unit of the Ferrovie dello Stato Group) that, in its role of Infrastructure Manager, is

82   responsible for the management and safety of the national rail traffic. With the aim of issuing real-time

83   earthquake alerts and measuring the shaking along the railway line, during a period of 3 years, we designed

84   and implemented a prototype EEW system on the high-speed railway between the cities of Rome and

85   Naples (hereinafter RM-NA line). The system is designed to be a support system for the management of

86   earthquakes in the railway environment. The RM-NA line extends for about 200km and runs almost

87   parallel and nearby to the central-south Apennine Mountain chain, which constitutes one of the highest

88   seismic areas of the country (Stucchi et al., 2004), where significant earthquakes (magnitude larger than

89   6.5) (Bernard & Zollo, 1989; Chiarabba et al., 2018; Chiaraluce, 2012; Galli & Galadini, 1999) have

90   occurred in the past (Fig. 1). The system is end-to-end, since it is fully customized to the specific

91   application it has been built for, being fully adapted and optimized to maximize its performance in terms of

92   speediness of the alert issuance and reliability of impact prediction, and thus, to account for the needs of the

93   railway infrastructure manager. It implements the most advanced scientific and technological solutions to

94   predict the expected ground shaking along the railway with the purpose of adopting operational restrictions

95   for slowing down or stopping the running trains approaching the potentially impacted portion of the line. It

96   concretizes the cutting-edge vision of EEW systems, in which the interaction with the end-user and the

97   interface with the target action play a key role in the design and configuration of the system itself (Cremen

98   & Galasso, 2020). Here we provide an overview of the system and describe the main elements and steps of

99   its implementation and operation. The core of our study is devoted to the description of an innovative,

100   quantitative performance evaluation that is presented together with general considerations and criteria

101   about the impact of the Early Warning system on the railway traffic along the pilot RM-NA High Speed

102   line that we believe should be considered in all designs of similar target applications.

103

104   2. DESIGN AND IMPLEMENTATION OF THE EARLY WARNING SYSTEM

105   *2.1 Seismic monitoring infrastructure development*

106   A dedicated seismic monitoring infrastructure was first developed. It is operated by RFI, with real-time

107   data acquisition and transmission capacity. The network consists of 20 stations installed on March 2020,

108   within the RFI Technological Sites located along the train line, covering the route from the northern

109   endpoint nearby Rome (Salone station) to the southern end-point nearby Naples (Afragola station) (Fig. 1).

110   Each station is equipped with a 3-component accelerometer, installed in a small buried superficial vault

111   (volume of about $1m^3$), specifically conceived to ensure the optimal coupling between sensor and ground

112   and to protect the sensor from high temperature variations. In 5 sites, an additional accelerometer is

113   installed at the bottom of a 20m-deep borehole, to improve the signal-to-noise ratio by reducing the

114   contamination of shallow noise ground vibrations. The installation of permanent stations was preceded by a

115   preliminary experimentation campaign aimed at the site characterization (in terms of quality of each

116   recording site, periodic noise-sources identifications, optimal sensor positioning). Text S1 of the

117   Supplemental Material shows examples of preliminary analyses for the site characterization (see also Fig.

118   S1 and S2 of the Supplemental Material).

119   The ground motion data is acquired at a frequency of 125 Hz (with 30bit-dynamic range data loggers),

120   georeferenced and synchronized via GPS, and transmitted in real-time to a central server (located in

121   Naples), through a dedicated, proprietary fiber optic telecommunication infrastructure managed by RFI.

122   The servers for calculation, data acquisition and storage are installed at Naples Central Station. Data

123   acquisition   from   the   stations   is   done   through   the   SeedLink   protocol

124   (http://ds.iris.edu/ds/nodes/dmc/services/seedlink/, last accessed January 2025), in the form of miniSeed

125   packets with a fixed size of 512 bytes and a fixed time duration of 0.6 seconds, to minimize the latency in

126   data transmission (Fig. 2). The EEW method is implemented in a modular software platform whose block

127   diagram is shown in Fig. 2. The platform is named AlpEW (Array lineare per Early Warning) and the main

128   steps of the methodology are synthetically described in the following paragraphs.

129

130   *2.2.Earthquake detection and train discrimination*

131   At the arrival of raw ground motion data from the seismic network, an automatic picking algorithm (Filter

132   Picker) (Lomax et al., 2012) is first used to identify the occurrence of a transient signal with respect to the

133   background noise. The most recurrent recorded noise signal at the station sites to be discriminated against

134   the earthquake signal is the ground vibration excited by the high-speed train transit that occurs hundreds of

135   times per day on average due to the intense daily railway traffic. Therefore, a dedicated algorithm for train

136   transit detection has been developed (Train Marker, TM), which analyses 1.5 seconds of recorded signal

137   (after the transient trigger detection) at each recording station and allows discriminating the earthquake

138   signal from the ground vibrations caused by the train transit, through the analysis of amplitude and

139   frequency content of the signals (see *Appendix A: Train Discrimination*). The TM parameter is built in a

140   way that signals with a dominant low frequency energy content (<15 Hz), such as seismic events, are

141   associated to small TM values, while the high frequency signals, such as those produced by the train

142   passage or other sources of noise, are generally associated to large TM values, although a clear separation

143   of TM values between trains and earthquakes does not exist (Fig. S3 in the Supplemental Material).

144

145   *2.3 Peak Ground Acceleration prediction*

146   When, at a given station, a potential P-wave pick originated by an earthquake is detected, its initial peak

147   acceleration (P_a), velocity (P_v) and displacement (P_d) amplitudes are measured in consecutive 1-sec time

148   windows after the first P-arrival time on the vertical component of ground motion up to a maximum time

149   window of 5 sec. The observed P-motion peak amplitudes at each site are used to predict the expected Peak

150   Ground Acceleration (PGA_{pred}) at each site, using predefined, empirical ground motion prediction

151   equations (see *Appendix B: Peak Ground Acceleration prediction*). Ground motion prediction equations are

152   often affected by large uncertainties, reflecting the natural variability and scatter of data, and which may

153   result in wrong estimates of the predicted quantities. Here we propose a probabilistic decision scheme for

154   the alert declaration which accounts for the probability of exceedance of a given PGA threshold value

155   (PGA_{th}), considering the uncertainty associated with the empirical scaling relationships. For each value of

156   observed P_d (P_v, or P_a) the corresponding, predicted PGA value (PGA_{pred}) is first computed from the

157 empirical scaling relationship. Then, an Exceedance Probability Level (EPL) is set to quantify to what

158 extent (with which confidence level) the predicted PGA will exceed the threshold level (PGA_{th}), accounting

159 for the uncertainties on scaling relationships. If the predicted PGA, considering the EPL threshold, exceeds

160 the PGA_{th}, the alert system is activated (Fig. S4 of the Supplemental Material). On the contrary, if the

161 predicted PGA, considering the EPL threshold, does not exceed the PGA_{th}, no action is taken by the system

162 (Fig. S4 of the Supplemental Material). Through the definition of the Exceedance Probability Level (EPL),

163 the system evaluates to what extent the predicted PGA will exceed the user-set threshold level (PGA_{th}),

164 accounting for the uncertainties on predictions (see *Appendix B: Peak Ground Acceleration prediction*).

165

166 *2.4 Decision Module and criteria for first alert declaration*

167 The probabilistic scheme described above is used at each recording site to establish the exceedance or not

168 of a given threshold value (PGA_{th}) on the predicted PGA. A Decision Module (DM) finally declares the

169 alert at the nodes of the line where the PGA_{th} is exceeded either by the predicted PGA, or by the recorded

170 acceleration on horizontal sensor components, whichever condition comes first. The DM implements

171 different configurations for the issuing of the first alert, requiring from a single node to multiple nodes

172 (max 4) to exceed the threshold in a user-defined time window, and accounting for space and time

173 coincidence criteria (Le Guenan et al., 2016; Minson et al., 2019), as described below and schematically

174 shown in Fig. S5 of the Supplemental Material:

175 *Single Station Basic alert (SSB)*: the system declares an alert as soon as $PGA_{pred} \geq PGA_{th}$ at one station;

176 *Single Station Refined alert (SSR1 - SSR2)*: the system declares an alert when $PGA_{pred} \geq PGA_{th}$ at one

177 station and $PGA_{pred} \geq PGA_{thmin}$ at one or two adjacent stations, respectively, being PGA_{thmin} a second lower

178 threshold on PGA.

179 *Multi Station alert (MS)*: the release of the alert occurs if $PGA_{pred} \geq PGA_{th}$ at N stations (with N going from

180 2 to 4) meeting specific time and space criteria, based upon the P-wave propagation. Specifically, the

181 relative spatial distances of the stations, $\Delta x(N)$, and temporal time differences of the picks, $\Delta t(N)$, are

182 checked for consistency with the propagation of seismic waves: the apparent velocities of the N picks

183 above threshold, calculated from the first pick, must be within a physically acceptable range.

184 The system is conceived to be evolutionary so that, even if the condition for the first alert release is not

185 satisfied at a certain time, the same condition may be fulfilled at later times.

186

187 2.5. *Emergency actions on the railway*

188 When the alert is declared by the DM, the "Alerted Segment of the Railway" (ASR) is the section of the

189 railway where $PGA_{pred} \geq PGA_{th}$. During the alert, the evolutionary ASR is computed and is continually

190 updated as long as the earthquake magnitude is updated and provided as output. Potential initial

191 underestimations, even at the two extreme segments of the line, can therefore be automatically corrected

192 when longer portions of the P-wave time windows and more stations are used and are automatically

193 recovered in the following seconds after the first alert declaration. Finally, it is worth mentioning that the

194 segment of the railway where operational restrictions are recommended is evaluated as the segment

195 comprising the nodes that issued alert, extended with an additional branch at the edge nodes, for caution.

196 No information is communicated at the non-triggered nodes.

197

198 2.6 *Integrated Earthquake Early warning and High-Speed Train Braking and Emergency Management*

199 *System*

200 The protocol for high-speed train braking system management follows the European Train Control System

201 (ETCS) (Rados et al., 2010) that works as part of the broader European Rail Traffic Management System

202 (ERTMS) (Laroche & Guihéry, 2013) to ensure safe and efficient operation of trains, including high-speed

203 traffic. The European Train Control System (ETCS) manages train movements and braking through a

204 combination of continuous communication, onboard computing, precise monitoring, and centralized control

205 (Flammini, 2010). The system relies on GSM-R (Global System for Mobile Communications - Railways)

206 for uninterrupted communication between the train and the control center, known as the Radio Block

Center (RBC). The RBC centralizes information on train movements and headway (the safe distance between consecutive trains) and issues movement authorizations. Each train is equipped with an onboard European Vital Computer (EVC), which processes data such as train speed, position, and status, as well as inputs from the RBC, to calculate train behaviour, including movement and braking strategies.

To ensure accurate positional data, Eurobalise transponders placed along the tracks provide precise position and speed information to the train. When a train passes over a Eurobalise, updated data is transmitted to the EVC to enhance accuracy. Using this real-time information—such as train speed, headway, distance to the next target, and safety parameters—the system calculates the optimal braking strategy.

The braking actuator (or emergency closure device) is then triggered to ensure the train stops precisely before the designated stopping point. The RBC continuously monitors train positions and enforces movement limits to prevent collisions, enabling trains to brake intelligently and stop safely at target points like signals or platforms. The emergency closure devices along a railway line are designed to quickly interrupt train operations in response to safety-critical situations, such as accidents, infrastructure failures, or hazards on the track. It can be activated manually by authorized personnel, such as railway operators or staff at a control center, or automatically by connected systems detecting anomalies like derailments, track obstructions, or signalling failures.

In the project of seismic early warning system development of Italian high-speed railways, specific emergency closure devices have been designed and built to be interfaced and remotely controlled by the seismic early warning system so to automatically activate the train stopping signal along the RM-NA railway. Once activated, the device sends an immediate signal to the railway signalling system, indicating that operational restrictions must be applied in the affected section of the track. This signal may also alert the centralized control center, allowing operators to coordinate further operational measures.

The electronic communications through GSM-R in ETCS-equipped railways transmit the emergency status directly to the onboard systems of trains, instructing them to stop. Approaching trains receive the emergency signal and initiate braking procedures; in automatic or semi-automatic systems, the train's

232 braking system is triggered immediately without requiring driver intervention, ensuring all trains within or

233 approaching the affected section come to a stop. Once the emergency closure is activated, the section of the

234 railway line is marked as out of service in the control system, preventing further train movements until the

235 issue is resolved. This process also triggers protocols for emergency response teams to assess and address

236 the situation and inspect the line. After the issue is resolved, the emergency closure device must be reset

237 manually or electronically by authorized personnel, and normal train operations can resume once the area

238 has been inspected with a positive outcome. In our integrated early warning and train traffic system, the

239 message of "end of earthquake emergency" is declared by the seismic early warning system that pilots the

240 automatic or semi-automatic deactivation, of the along-line emergency closure devices.

241

242 *2.7. Graphical User Interface (GUI)*

243 Finally, the EEW platform further outputs its analyses and results in a Graphical User Interface (GUI) for

244 RFI's control room, which displays the main parameters provided by the system in real-time, some

245 statistics over set time windows (12-hour, 7 days), portion of the lines where operational restrictions have

246 been applied. In the post-event, the GUI allows an operator to evaluate the performance of the system in

247 terms of measured parameters and output release and to promptly identify any relevant anomalies (such as

248 the absence of data from a station or the presence of anomalous noise records), which is useful for prompt

249 intervention and maintenance.

250
251

252 3. PERFORMANCE EVALUATION

253 3.1 *Offline analysis of system performance*

254 A quantitative evaluation of the performance of the EEW system is crucial for stakeholders and end-users

255 (Le Guenan et al., 2016) to setup the operational system and properly configure the several configuration

256 parameters, including, for instance, the PGA_{th} threshold value and the minimum number of nodes at which

257 the predicted PGA should exceed this value to declare the warning. Due to the absence of a massive

258   catalogue of real earthquake waveforms recorded at the high-speed railway sites, the performance here is

259   evaluated through a retrospective, off-line analysis of the system outputs, for a massive number of offline

260   playbacks of earthquake records at the AlpEW system, as explained in the following paragraphs.

261   The database for performance evaluation includes both real earthquake waveforms (sorted from the

262   waveform databanks of Italian earthquakes) and train transit signals (effectively recorded at stations along

263   the RM-NA line). We identified 2 linear arrays of stations from the Italian National Accelerometric

264   Network (RAN) (Gorini et al., 2010). The arrays have been specifically selected to simulate at best the

265   geometry, extension (total length about 200 km), orientation and spacing of the sensors, as compared to the

266   RFI nodes, as well as their relative position with respect to the source area. The arrays are selected by the

267   National Accelerometric Network (RAN) and are located in Central Italy, in the Apennine area, in a near-

268   parallel and near-orthogonal orientation with respect to the Apennine chain itself. Fig. S6 of the

269   Supplemental Material shows the networks used for the experimentation, the relative stations and the

270   epicentral positions of the earthquakes. A total of 56 seismic events and 975, 3-component records were

271   selected (i.e., 325 records for each component). The complete earthquake database is composed as follows:

272   *Apennine Array*: 16 stations, 28 earthquakes with magnitudes between 3.5 and 6.5;

273   *Anti-Apennine Array*: 12 stations, 28 earthquakes with magnitudes between 3.5 and 6.5;

274   We also evaluated the impact of the train transits on the system performance by simulating the partial and

275   total overlapping of their signals with the P-wave recordings. We extracted random samples of train transits

276   (acquired at the RFI nodes during an earlier phase of the project) and summed-up them to the earthquake

277   records, simulating a partial or total overlap with the P-wave. Fig. S7 illustrates an example of signal

278   obtained by adding the train passage record to a seismic event, before the arrival of the P-wave, in

279   acceleration, velocity and displacement (from top to bottom, respectively).

280   As for the simulation of different configuration parameters, here we explore three specific parameters

281   which are: the PGA_{th}, the EPL level and the DM configuration for the first alert release. We varied these

282   parameters in reasonable ranges (suitable for the Italian railway applications) and, for each combination of

283 the three parameters, we evaluated the response of the system. The complete list of the twenty-two

284 explored combinations (denoted by C) is shown in Table S3 of the Supplemental Material. Considering the

285 total number of available records (975) and the selected noise windows (7), a total of 6825 three-

286 component recordings (2275 records per single component) were generated.

287 For each of the configurations explored, we used all the available records to evaluate the performance.

288 Depending on the comparison between the predicted and the observed value of PGA (PGA$_{obs}$), four

289 different alert categories at each single node may occur:

290 SD (Successful Declaration of threshold exceedance):

291 $PGA_{pred} \geq PGA_{th} \ \& \ PGA_{obs} \geq PGA_{th}$ (1a)

292 SND (Successful No Declaration of threshold exceedance):

293 $PGA_{pred} < PGA_{th} \ \& \ PGA_{obs} < PGA_{th}$ (1b)

294 FD (False Declaration of threshold exceedance):

295 $PGA_{pred} \geq PGA_{th} \ \& \ PGA_{obs} < PGA_{th}$ (1c)

296 MD (Missed Declaration of threshold exceedance):

297 $PGA_{pred} < PGA_{th} \ \& \ PGA_{obs} \geq PGA_{th}$ (1d)

298

299 We then introduced a straightforward formulation for the performance assessment of the AlpEW system in

300 terms of two indicators: 1) the *Quickness Index QI(C)*, computed as:

301 $\underline{QI(C)} = \frac{\sum_{i=1}^{N_{alerts}} TFD_i(C)}{N_{alerts}};$ (2)

302 This parameter is defined as the mean value of TFD for each specific configuration C and represents the

303 rapidity of the system in providing first alerts. The QI is computed only for the events belonging to the

304 N$_{alerts}$ subset;

305   2) the *Impact Prediction Performance IPP(C,t)*, computed as:

306 $\underline{IPP(C,t)} = \frac{\sum_{j=1}^{N_{nodes}}[SD_j(C,t) + SND_j(C,t)]}{N_{nodes}} \cdot 100;$ (3)

307 This parameter represents the percentage of successful predictions of PGA (as the sum of $N_{SD} + N_{SND}$), at a

308 given time t and for a specific configuration C and it is evaluated for all available nodes for which the P-

309 wave signal is available at the considered time. It represents the EEW system ability to correctly predict/not

310 predict the ground shaking level at a single node.

311 In the above formula:

312 $\underline{N_{alerts}}$ is the number of earthquakes $PGA_{obs} \geq PGA_{th}$ at a variable number of nodes (depending on the

313 configuration C); $\underline{N_{nodes}}$ is the total number of available nodes considering all networks and performed

314 simulations (it is the same for each configuration C and is equal to 2275); $\underline{TFD\ (C)\ is}$ the time of the first

315 declaration of threshold exceedance, measured in seconds since the first P-wave detection at the network,

316 for each event of the subset defined by $N_{alerts,}$ i.e, those events for which the observed PGA has exceeded

317 the threshold value at least in one node of the network.

318 For each configuration of the three explored parameters (PGA_{th}, DM, EPL), we computed the median

319 values of QI and IPP as obtained from the playbacks. A useful way of representing the performance is

320 provided by the IPP vs. QI diagram of Fig. 3. The proposed scheme allows positioning each configuration

321 in the ideal space of the two indicators and provides an immediate and quick visualization of the system

322 performance. The best performing configurations are those that maximize the IPP parameter while

323 minimizing the QI value (top-left diagram corner). For clarity of representation, in Fig. 3, we did not

324 associate each configuration with a different symbol, but we highlighted behavior of the system depending

325 on DM, PGA_{th} and EPL values.

326 The performance analysis is summarized in Fig. 3 for all events (panels a, c) and *relevant* earthquakes only

327 (panels b, d), where a "*relevant*" earthquake is defined as an event for which the observed PGA has

328 exceeded the user-set threshold at least in one node of the network. The performance is shown at the Time

329 of the First Declaration of threshold exceedance (TFD) (panels a, b), and 5 seconds later (TFD+5) (panels

330 c, d) for all events (panels a, c) and for relevant earthquakes only (panels b, d). For all the tested

331 configurations, the first alert declaration (TFD) is typically released within a short time after the first P-

332   detection at the network, in a range of 3 to 8 seconds for all earthquakes, and 3 to 10 seconds for relevant

333   earthquakes. At these times, the IPP parameter ranges between 85% and 97% of successes (positive and

334   negative successful alerts) for all events (Fig. 3a) and between 65% and 85% for relevant earthquakes (Fig.

335   3b). At later times, at TFD + 5s, the performance in terms of IPP varies between 90% and 100% for all

336   events (Fig. 3c) and between 80% and 93% for relevant earthquakes (Fig. 3d). For all configurations, the

337   use of high EPL values (75% or 90% (empty symbols) generally requires longer times to issue the first alert

338   declaration and does not provide significant performance improvements, as compared to the value EPL =

339   50% (filled symbols).

340   Whichever configuration is used, an increase of the user-set PGA_{th} generally results into a slightly higher

341   impact prediction performance, when considering all the events. This is a widely understood behaviour of

342   early warning systems and reflects the relative larger number of SND, with respect to the SD, when

343   increasing the threshold level for warning declaration (Minson et al., 2019). Indeed, the same effect is less

344   evident when considering the relevant earthquakes only, for which the number of SD remains rather

345   constant between different configurations, and SND are partially reduced from the computation. The

346   threshold-dependency of impact prediction performance becomes less evident at later times.

347   It is worth to mention that the percentages here refer to the individual node numbers that provide successful

348   declarations (both SD and SND) vs. unsuccessful declarations (both MD and FD). This means that, in case

349   of a missed/false declaration of threshold exceedance at a single node, there will be an

350   underestimation/overestimation of the railway segment length affected by strong shaking, but anyway the

351   alert for a potential damaging earthquake occurrence will be issued in most of the cases. The

352   underestimation of the railway segment length affected by strong shaking is mitigated by considering a

353   buffer zone at the beginning and at the end of the segment.

354

355

356

3.2 *Real-time system monitoring*

During the period March 2020-January 2022, the EW system has been running in real-time at the RFI railway to test the whole operational chain from data acquisition, transmission, and analysis. The AlpEW system was configured to run with the SSRA decision module, with PGAth set to 10%g for the central station and to 5% of g for the two adjacent stations.

Together with the real-time software running, we carried out a daily monitoring activity during working days (Mon-Fri), through remote connection to the servers at "Napoli Centrale" train station, with the main goal of checking the state-of-health of the EW system, including both the physical infrastructure and the software components. The daily monitoring procedures included a visual inspection of the system status (through dedicated monitors) and the analysis of specific parameters, which are automatically computed and stored in a dedicated file. On a daily basis, we essentially monitored: the number of working stations; the presence of gaps or delays in data transmission at each station (and the potential lost minutes of signals); the quality of recorded signals (in terms of minimum and maximum recorded PGA); the presence of noise transients and, finally, the performance of the EW software in case of earthquake detections.

During this period, 9 earthquakes with magnitude ranging between 2 and 3.4 have occurred at minimum distances from the rail of 10-20 km. None of the recorded earthquake triggered the alert declaration at the network sites, with all the PGA_{pred} being correctly smaller than the threshold value at all nodes. As an example, Figure S8 shows the position (with respect to the network infrastructure) of the largest recorded event with magnitude ML 3.4 on 2021-06-22 at 18:37:04 (http://terremoti.ingv.it/event/27189251) and summarizes the performance of the EW system in terms of parameter estimates, Decision Module and Alert Declaration.

379 4. DISCUSSION

380 We presented here the first, end-to-end EEW system operating along the high-speed railway between

381 Naples and Rome in Italy. The system has been conceived and developed to be fully target-oriented,

382 incorporating dedicated methodologies for the impact evaluation and customized strategies for alert release.

383

384 *4.1 Innovation of the proposed Earthquake Early Warning system for High-Speed Railway Seismic*

385 *management*

386 The earthquake early warning (EEW) system developed for high-speed railway infrastructure in Italy

387 represents a groundbreaking advancement in both seismology and railway control technologies. Unlike

388 traditional offline applications and testing of EEW methodologies, this work pioneers the first operational

389 system specifically designed for the high-speed Italian railway network. High-speed trains, travelling at

390 several hundred kilometers per hour, require cutting-edge signaling and control systems to ensure fast

391 interventions and operational efficiency. Thanks to the successful results obtained during the

392 implementation of this pilot project RFI decided to expand Earthquake Early Warning systems to other

393 high-speed lines of the national network.

394 The innovation of this system is multifaceted: it integrates P-wave and S-wave data to assess potential

395 impacts, moving beyond conventional source-based early warning approaches. Additionally, it combines

396 network-based and on-site decision-making using probabilistic, evolutionary approaches that continuously

397 refine alerts as seismic data becomes available. The robust processing capabilities leverage accelerometric,

398 velocimetric and displacement signals to ensure high-frequency range coverage, allowing precise and

399 reliable seismic analysis. A standout feature of the system is its ability to define geographically targeted

400 alert zones, avoiding unnecessary shutdowns and enabling operation on unaffected segments - a stark

401 improvement over other systems that may enforce the traffic arrest along wide-impacted railway line

402 (Yamamoto & Tomori, 2013). Moreover, the project introduces a technological leap by automating the

403 railway emergency closure mechanisms, transitioning from manual to remote operations with real-time

404 functionality. This operationalization of EEW for railways not only exemplifies innovation but also sets a

405 new benchmark for integrating earthquakes management into critical transportation infrastructures.

406

407 *4.2 System performance evaluation*

408 For a distributed target such as the railway line, the traditional concept of magnitude estimation accuracy

409 and lead-time are, indeed, not applicable. The effectiveness of an EEW system should therefore be

410 evaluated in a broader sense. Here we first propose a compact and powerful diagram which transforms the

411 classical approach to the performance evaluation and allows end-users to choose the optimal system

412 configuration parameters. We then evaluate the impact of the system on the railway traffic of the whole

413 line, accounting for the actual probability of occurrence of potentially relevant earthquakes.

414 The EEW system for high-speed railways in Italy is evolutionary in time, meaning that PGA predictions are

415 updated as the P-wave propagates across the network. However, the Decision Module (DM) is conceived in

416 a way that once the declaration of threshold exceedance is given at any node, the step back is no longer

417 possible during the seismic shock. Indeed, the definitions of SD (Successful Declaration), SND (Successful

418 No Declaration), FD (False Declaration) and MD (Missed Declaration) are based on the comparison

419 between predicted and observed PGA values. While the PGA prediction may evolve with time as longer

420 portions of P-wave signals are analyzed, the *a-posteriori* observed value of PGA is fixed. Moreover, the

421 expected PGA is continuously predicted from the initial P-wave peak amplitude (P_d, P_v, P_a) which are

422 computed as the absolute maximum amplitude in increasing P-wave time windows, in displacement,

423 velocity and acceleration, respectively. Therefore, the prediction can only increase or remain stable with

424 time. In other words, once the predicted PGA has exceeded the threshold value, the warning declaration

425 cannot be cancelled during the seismic shock. With this in mind, the prediction performance at any node

426 may potentially evolve with time from SND to FD or from MD to SD. Other transitions between alert states

427 are indeed not possible. Thus, a way to improve the quality of predictions and maximize the real-time

428 performance is by reducing FD since the first alert, with more robust P-amplitude to PGA prediction

429   models, accounting for a more comprehensive approach for all source, propagation, and site effects.

430   Additionally, the experience of operational or under testing EEW systems worldwide teaches us that: 1) the

431   performance of a system in terms of correct or wrong predictions of the PGA strongly depends on the

432   threshold value for the alert declaration; 2) the declaration of correct alerts can be pushed to the limits,

433   while the trade-off between missed and false alerts cannot be eliminated (Minson et al., 2019). Indeed, the

434   lower the threshold is, the higher is the probability for the system of issuing false alerts, with a relatively

435   small number of missed alerts. Conversely, if a high threshold is requested to release the warning, the

436   chance of declaring false alerts decreases, but the incidence of missed alerts may increase.

437

438

439   *4.3 Alerted Segment of the Railway (ASR) and Potential Benefits of the Early Warning System*

440   Beyond performance evaluation, a critical aspect of this study is the utilization and effectiveness of

441   earthquake alerts in railway applications (Minson et al., 2021). Stopping a high-speed train completely

442   requires a considerable amount of time, which may sometimes exceed the warning time provided by the

443   system. Therefore, one of the primary advantages of the EEW system is its ability to prevent high-speed

444   trains from entering the Alerted Segment of the Railway (ASR) while promptly initiating deceleration for

445   trains already within the segment. This approach helps mitigate the potential impacts of seismic shocks.

446   During an earthquake alert, operational restrictions would slow down and eventually stop trains within the

447   ASR, while preventing entry for trains approaching the segment from either direction.

448   The proportion of trains inside or outside the ASR during an alert depends on train traffic density along the

449   railway and the extent of the ASR, which is determined by the earthquake's magnitude (M) and its distance

450   (R) from the railway line. We computed the expected ASR lengths for earthquakes with magnitudes

451   between 4.5 and 7, occurring at distances of 10 to 100 km from the RM-NA railway line, using an

452   empirical relation, similar to a standard GMPE, between the length of ASR, the earthquake magnitude (M)

453   and the distance of the earthquake from the railway (R) (see *Appendix C:Alerted Segment of the Railway*

454   *computation*). Figure 4 shows data used for the estimation of the ASR. Additionally, a two-month analysis

455   of train traffic on the high-speed railway revealed two occupancy patterns: low-density periods (6:00–10:00

456   and 20:00–23:00) and high-density periods (10:00–20:00), during which rail occupancy remains relatively

457   consistent across the line (Fig. 5a). Based on these occupancy trends and earthquake scenarios, we

458   estimated the distribution of trains inside and outside the ASR, as shown in Fig. 5b. For most ASR lengths

459   and time periods, the percentage of trains outside the ASR exceeds those within it, except for the case

460   where ASR = 100 km, where the proportions are approximately equal. An ASR length of 100 km

461   corresponds to a large earthquake occurring close to the railway line (M > 6.5, R < 20 km). This represents

462   a rare scenario for the RM-NA railway, with an estimated return period of approximately 2,000 years (Fig.

463   5c) (*Appendix C:Alerted Segment of the Railway computation*). More frequent cases, with return periods of

464   10–15 years, involve moderate earthquakes (M 4–5) occurring within 10–20 km of the railway, resulting in

465   ASRs of about 10 km. In these instances, the vast majority of trains would likely receive sufficient warning

466   to decelerate or stop before entering the ASR.

467   Furthermore, while the current ASR estimates rely on theoretical PGA values, the ability of the EEW

468   system to rapidly identify non-relevant earthquakes or adjust ASR parameters based on real-time data could

469   significantly enhance the system's efficiency. This would enable faster resumption of train operations,

470   providing substantial benefits to the overall railway infrastructure.

471

472   *4.4 Early Warning System Exportability*

473   A significant aspect of this work is the scalability and adaptability of the proposed early warning system

474   beyond the pilot line. The platform has been designed with exportability in mind, making it readily

475   applicable to other segments of the national railway network. This flexibility is critical for extending the

476   benefits of the system to a broader range of railway infrastructures, particularly in seismically active

477   regions.

478   The system can be seamlessly integrated with any existing seismic network, whether linear or spatially

479   distributed, provided that the network supports real-time data acquisition and transmission. Once deployed,

480   the platform can process incoming data from these networks to deliver precise earthquake locations and

481   generate accurate near real-time shake maps. These capabilities are crucial not only for issuing timely alerts

482   but also for coordinating rapid post-event response actions, such as infrastructure inspections and traffic

483   management. Furthermore, the ability to generate reliable shake maps in near real-time allows railway

484   operators to assess the impact of seismic events on specific segments of the infrastructure. This targeted

485   approach ensures that traffic can be quickly resumed on unaffected sections of the railway line, minimizing

486   disruptions and reducing downtime. The system's modular design also enables customization to meet the

487   specific requirements of different railway networks, accommodating variations in seismic hazard levels,

488   infrastructure layouts, and operational priorities.

489

490   *CONCLUSIONS*

491   This study presents the development and implementation of the first fully operational Earthquake Early

492   Warning (EEW) system specifically designed for high-speed railway infrastructure in Italy. Implemented

493   along the Naples-Rome high-speed railway line in Italy, the system embodies a significant technological

494   and methodological leap in both seismic management and railway operations. It offers a practical and

495   highly effective solution for mitigating the risks posed by earthquakes in critical transportation networks:

496   -   Unlike traditional EEW approaches that focus solely on source parameters, this system integrates P-

497   wave and S-wave data to evaluate potential impacts dynamically and adopts an evolutionary

498   decision-making approach. This ensures that alerts are continuously refined as seismic data

499   becomes available, improving accuracy and response times.

500   -   Its ability to define geographically specific alert zones minimizes unnecessary disruptions by

501   isolating affected railway segments, a stark contrast to conservative systems that may necessitate

502   total line shutdowns. Furthermore, the integration of automated emergency closure mechanisms

503   enhances operational efficiency and reliability by enabling remote, real-time control of railway

504   traffic during seismic events.

505 -   The performance evaluation of the system demonstrates its robustness and adaptability to the unique

506   challenges posed by high-speed railways. The system accounts for the complexities of train

507   occupancy patterns, seismic event parameters, and the spatial distribution of seismic networks. By

508   preventing trains from entering the Alerted Segment of the Railway (ASR) and initiating controlled

509   deceleration for those within it, the system effectively mitigates seismic impacts.

510 -   The platform's design is inherently scalable and exportable, making it applicable to other segments

511   of the national and international railway networks. Its seamless integration with existing seismic

512   networks enables precise earthquake location and near real-time shake map generation, essential for

513   coordinating post-event responses.

514

515

516

517 *Appendix A:Earthquake detection and train discrimination*

518 The TM parameter is a linear combination of the form:

519 $$TM = \alpha \log(P_a/P_d) + \beta \log(1/\tau_c) + \gamma \log(RUD) \quad (4)$$

520 where:

521 P_a and P_d are the absolute maximum amplitude on acceleration and displacement waveforms, respectively,

522 measured on the vertical components in a short time window after the P-wave arrival; τc is the

523 characteristic (or dominant) period of the signal (Kanamori, 2005); RUD (Iwata et al., 2015) expresses the

524 ratio between the acceleration signal, filtered in the high-frequency band (15-40 Hz) and the acceleration

525 signal, filtered in the low-frequency band (0.075-3 Hz); α, β, γ are empirical coefficients. The signals with

526 a dominant low frequency energy content (<15 Hz), such as seismic events, are associated to small TM

527 values, while the high frequency signals, such as those produced by the train passage or other sources of

528 noise, are generally associated to large TM values, although a clear separation of TM values between trains

529 and earthquakes does not exist (Fig. S3 in the Supplemental Material). The coefficients α, β, γ, are

530 estimated for each station using a global exploration algorithm and are chosen as the values that maximize

531 the discrimination capability of the TM parameter (i.e., those parameters that minimize the overlap of TM

532 distributions, between train signals and earthquake records). The α, β and γ values, as well as the threshold

533 value on TM parameter for each station reported in Table S1 of the Supplemental Material.

534 The discrimination algorithm finally requires an additional constraint on the amplitude level of the recorded

535 signal, to discard other potential sources of noise (such as electromagnetic or lightning interferences) that

536 may produce ground vibrations and interfere with seismic signals. A seismic event is declared when either

537 $TM < TM_{th}$ or when $P_d > P_{dth}$, being TM_{th} and Pd_{th} prior established threshold levels on the two parameters,

538 respectively. The threshold value on the logarithm of P_d is set for all stations to -2.16 (cm), which

539 corresponds to an Intensity (IMCS) equal to III, when log P_d is scaled to the Peak Ground Acceleration

540 (PGA) through the empirical relationship from Faenza & Michelini (2010) as explained in the following

541 section.

542 We point out that there are currently several literature papers supporting the use of ML classification and

543 discrimination algorithms for seismic signals, as well as for the prediction of ground motion quantities

544 (Choi et al., 2024; Li et al., 2023; J. Zhu et al., 2024). While the identification of train generated signals

545 may be accomplished machine learning algorithms, the challenge for an EW system is to be able to

546 discriminate the earthquake from the train signals using a very short time window (of the order of 1

547 second). To our knowledge, there are no consolidated examples of machine learning algorithms specifically

548 tailored for detecting and picking P-wave arrivals along railway lines.

549

550

551 *Appendix B: Peak Ground Acceleration prediction*

552 The observed P-motion peak amplitudes at each site are used to predict the expected Peak Ground

553 Acceleration (PGA$_{pred}$), which represents the standard parameter for seismic vulnerability assessments in

554 railways applications (Nakamura, 1988; Nakamura & Saita, 2007). The PGA is predicted from the initial

555 peak amplitude parameters using empirical ground motion prediction equations relating the initial

556 amplitude of the P-wave to the maximum acceleration level of the form:

$$\log PGA = a + b \log(P_x) \quad (5)$$

558 where P_x represents the initial peak amplitude in displacement, velocity, or acceleration (P_d, P_v, P_a,

559 respectively), a and b are empirically derived coefficients (and related uncertainties) for each specific time

560 window from 1.5 to 5 seconds, and PGA is the absolute maximum among the two horizontal components.

561 Equation 5 is used in real-time operations to predict the PGA as the weighted average between the three

562 estimates from P_d, P_v, P_a. For each value of observed P_d (P_v or P_a) the corresponding, predicted PGA value

563 (PGA_{pred}) is first associated to a log-normal distribution, centred at the log-PGA_{pred} value and with a width

564 given by the standard deviation of the empirical scaling relationship (Fig. S4 of the Supplemental Material

565 Then, an Exceedance Probability Level (EPL) is set to the log-normal distribution, to quantify to what

566 extent (with which confidence level) the predicted PGA will exceed the threshold level (PGA^{th}). Weights

567 are inversely proportional to the standard error of each scaling relationship (defined by equation 2) and the

568 final variance (σPGA_{pred}) is given by the standard propagation of the errors on the three estimated

569 quantities. The coefficients a and b are calibrated on a database of Italian earthquakes occurred between

570 2009 and 2016, with magnitude between 3.5 and 6, available from the Department of Civil Protection

571 through the ITACA 2.0 Portal (Luzi et al., 2008). The table containing all coefficients for each parameter

572 and each time window is provided in Table S2 of the Supplemental Material.

573 The use of three peak-amplitude parameters has already been discussed in literature (Colombelli et al.,

574 2015) and has been shown to improve the PGA predictions, with respect to the use of a single amplitude

575 parameter, since the three quantities are related to different frequency bands of the recorded ground motion

576 and thus their combination allows for a more broad-band characterization of the earthquake ground motion.

577 The maximum time window of 5 seconds has been chosen according to the expected maximum P-

578 displacement half-duration for moderate to large earthquakes (M about 7) in Italy as inferred from

579   theoretical and observed rupture duration vs seismic moment scaling relationships (Sato & Hirasawa,

580   1973).

581

582

583   *Appendix C:Alerted Segment of the Railway computation*

584   To predict the extension of the ASR, we derive an empirical relation, similar to a standard GMPE, between

585   the length of ASR, the earthquake magnitude (M) and the distance of the earthquake from the railway (R).

586   To this purpose, we simulated the seismicity of the area (in terms of earthquake locations and magnitudes),

587   through the seismogenic zones of the Italian seismic hazard model MPS04 (Stucchi et al., 2004). We

588   generated a massive distribution of events in a maximum distance of 200 km from the railway, for a total of

589   100 catalogs, each simulating 100 years of seismicity. Then, for each event, we computed the PGA_{pred}

590   along the RM-NA railway, using the empirical attenuation relation from Bindi et al. (2011) and estimated

591   ASR as the portion of the line in which $PGA_{pred} \geq PGA_{th}$ defines the length of the ASR. This estimated

592   length is finally correlated to the earthquake magnitude and distance from the line (Fig. 4b) using the

593   following model:

594   $$log_{10} \text{ASR} = A \cdot log_{10} R + B \cdot M + C \pm \sigma \quad (6)$$

595   where R is measured in km, ASR is in km and A, B, and C are empirically estimated coefficients. We

596   found A= -0.54 ± 0.04, B= 0.64 ± 0.02, C=-1.82 ± 0.08, σ=0.24.

597   To estimate the impact in terms of train transit, we counted the number N of trains that exceeded a given

598   threshold in impacted length. The return period is then computed as: RP = (1000 ·100 years)/N.

599

600

601

602

603

604

Author Contribution

S. Colombelli, Conceptualization, Methodology, Writing- Reviewing and Editing; **A. Zollo,** Conceptualization, Methodology, Writing- Reviewing and Editing, Supervision, Funding acquisition; **L. Elia,** Methodology, Software, Writing- Reviewing and Editing; **G. Festa,** Methodology, Writing- Reviewing and Editing; **G. Iannaccone,** Methodology, Writing- Reviewing and Editing; **M. Picozzi,** Methodology, Writing- Reviewing and Editing; **A. Caruso,** Methodology, Formal analysis, Data Curation, Writing- Reviewing and Editing; **F. Carotenuto**, Formal analysis, Data Curation, Writing- Reviewing and Editing; **S. Gammaldi,** Formal analysis, Data Curation, Writing- Reviewing and Editing; **A. G. Iaccarino,** Methodology, Formal analysis, Data Curation, Writing- Reviewing and Editing; **R. Riccio,** Formal analysis, Data Curation, Writing- Reviewing and Editing; **S. Tarantino,** Methodology, Formal analysis, Data Curation, Writing- Reviewing and Editing; **A. Mauro,** Conceptualization, Methodology, Writing- Reviewing and Editing; **G. Polimanti,** Conceptualization, Methodology, Writing- Reviewing and Editing; **F. Cirillo,** Methodology, Writing- Reviewing and Editing; **A. Vecchi,** Methodology, Writing- Reviewing and Editing; **F. Iacobini,** Conceptualization, Writing- Reviewing and Editing.

Acknowledgment

Data and materials availability: Earthquake acceleration waveforms used in this study were collected from the Italian Accelerometric Archive (ITACA) 3.1 (D'Amico et al., 2020; Pacor et al., 2011) at http://itaca.mi.ingv.it (last accessed January 2025). Train passages have been recorded at proprietary stations of the Italian Railway Company (RETE FERROVIARIA ITALIANA S.p.A).

References

Allen, R. M., & Melgar, D. (2019). Earthquake early warning: Advances, scientific challenges, and societal needs. In *Annual Review of Earth and Planetary Sciences* (Vol. 47, pp. 361–388). Annual Reviews Inc. https://doi.org/10.1146/annurev-earth-053018-060457

Bernard, P., & Zollo, A. (1989). The Irpinia (Italy) 1980 earthquake: Detailed analysis of a complex normal faulting. *Journal of Geophysical Research: Solid Earth*, *94*(B2), 1631–1647. https://doi.org/10.1029/JB094IB02P01631

Bindi, D., Pacor, F., Luzi, L., Puglia, R., Massa, M., Ameri, G., & Paolucci, R. (2011). Ground motion prediction equations derived from the Italian strong motion database. *Bulletin of Earthquake Engineering 2011 9:6*, *9*(6), 1899–1920. https://doi.org/10.1007/S10518-011-9313-Z

Chiarabba, C., De Gori, P., Cattaneo, M., Spallarossa, D., & Segou, M. (2018). Faults Geometry and the Role of Fluids in the 2016–2017 Central Italy Seismic Sequence. *Geophysical Research Letters*, *45*(14), 6963–6971. https://doi.org/10.1029/2018GL077485

Chiaraluce, L. (2012). Unravelling the complexity of Apenninic extensional fault systems: A review of the 2009 L'Aquila earthquake (Central Apennines, Italy). *Journal of Structural Geology*, *42*, 2–18. https://doi.org/10.1016/J.JSG.2012.06.007

Choi, S., Lee, B., Kim, J., & Jung, H. (2024). Deep-Learning-Based Seismic-Signal P-Wave First-Arrival Picking Detection Using Spectrogram Images. *Electronics 2024, Vol. 13, Page 229*, *13*(1), 229. https://doi.org/10.3390/ELECTRONICS13010229

Clinton, J., Zollo, A., Marmureanu, A., Zulfikar, C., & Parolai, S. (2016). State-of-the art and future of earthquake early warning in the European region. *Bulletin of Earthquake Engineering*, *14*(9). https://doi.org/10.1007/s10518-016-9922-7

Colombelli, S., Caruso, A., Zollo, A., Festa, G., & Kanamori, H. (2015). A P wave-based, on-site method for earthquake early warning. *Geophysical Research Letters*, *42*(5), 1390–1398. https://doi.org/10.1002/2014GL063002

Cremen, G., & Galasso, C. (2020). Earthquake early warning: Recent advances and perspectives. In *Earth-Science Reviews* (Vol. 205). Elsevier B.V. https://doi.org/10.1016/j.earscirev.2020.103184

Cremen, G., Galasso, C., & Zuccolo, E. (2022). Investigating the potential effectiveness of earthquake early warning across Europe. *Nature Communications 2022 13:1*, *13*(1), 1–10. https://doi.org/10.1038/s41467-021-27807-2

D'Amico, M. C., Felicetta, C., Russo, E., Sgobba, S., Lanzano, G., Pacor, F., & Luzi, L. (2020). *ITalian ACcelerometric Archive (ITACA), version 3.1*. Istituto Nazionale Di Geofisica e Vulcanologia (INGV).

Erdik, M., Fahjan, Y., Ozel, O., Alcik, H., Mert, A., & Gul, M. (2003). Istanbul earthquake rapid response and the early warning system. *Bulletin of Earthquake Engineering*, *1*(1), 157–163. https://doi.org/10.1023/A:1024813612271/METRICS

European Commission. (2014). *Technology Readiness Levels (TRL). HORIZON 2020 – WORK PROGRAMME 2014-2015 General Annexes, Extract From Part 19 - Commission Decision C* .

Faenza, L., & Michelini, A. (2010). Regression analysis of MCS intensity and ground motion parameters in Italy and its application in ShakeMap. *Geophysical Journal International*, *180*(3), 1138–1152. https://doi.org/10.1111/J.1365-246X.2009.04467.X

Firmi, P., Iacobini, F., Rinaldi, A., Vecchi, A., Agostino, I., & Mauro, A. (2020). Methods for managing hydrogeological and seismic hazards on the Italian railway infrastructure. *Structure and Infrastructure Engineering*, *17*(12), 1651–1666. https://doi.org/10.1080/15732479.2020.1822883

Flammini, F. (2010). Sistemi di controllo per l'Alta Velocità ferroviaria. *Mondo Digitale*, *9*, 18–32.

Galli, P., & Galadini, N. F. (1999). Seismotectonic Framework of the 1997-1998 Umbria-Marche (Central Italy) Earthquakes. *Seismological Research Letters*, *70*(4), 417–427.

Gorini, A., Nicoletti, M., Marsan, P., Bianconi, R., De Nardis, R., Filippi, L., Marcucci, S., Palma, F., & Zambonelli, E. (2010). The Italian strong motion network. *Bulletin of Earthquake Engineering*, *8*(5), 1075–1090. https://doi.org/10.1007/s10518-009-9141-6

Iwata, N., Yamamoto, S., Korenaga, M., & Noda, S. (2015). Improved Algorithms of Seismic Parameters Estimation and Noise Discrimination in Earthquake Early Warning. *Quarterly Report of RTRI*, *56*(4), 291–298. https://doi.org/10.2219/RTRIQR.56.4_291

Kanamori, H. (2005). Real-time seismology and earthquake damage mitigation. *Annual Review of Earth and Planetary Sciences*, *33*, 195–214. https://doi.org/10.1146/annurev.earth.33.092203.122626

Lakušić, S., Haladin, I., & Vranešić, K. (2020). Railway infrastructure in earthquake affected areas. *Gradjevinar*, *72*(10), 905–921. https://doi.org/10.14256/JCE.2967.2020

Laroche, F., & Guihéry, L. (2013). European Rail Traffic Management System (ERTMS): Supporting competition on the European rail network? *Research in Transportation Business & Management*, *6*, 81–87. https://doi.org/10.1016/J.RTBM.2012.12.006

Le Guenan, T., Smai, F., Loschetter, A., Auclair, S., Monfort, D., Taillefer, N., & Douglas, J. (2016). Accounting for end-user preferences in earthquake early warning systems. *Bulletin of Earthquake Engineering*, *14*(1), 297–319. https://doi.org/10.1007/s10518-015-9802-6

684   Li, B., Fan, L., Jiang, C., Liao, S., & Fang, L. (2023). CSESnet: A deep learning P-wave detection model based on UNet++
685   designed for China Seismic Experimental Site. *Frontiers in Earth Science*, *10*, 1032839.
686   https://doi.org/10.3389/FEART.2022.1032839/BIBTEX
687   Lomax, A., Satriano, C., & Vassallo, M. (2012). Automatic picker developments and optimization: Filterpicker-A robust,
688   broadband picker for real-time seismic monitoring and earthquake early warning. *Seismological Research Letters*, *83*(3),
689   531–540. https://doi.org/10.1785/gssrl.83.3.531
690   Luzi, L., Hailemikael, S., Bindi, D., Pacor, F., Mele, F., & Sabetta, F. (2008). ITACA (Italian ACcelerometric Archive): A web
691   portal for the dissemination of Italian strong-motion data. *Seismological Research Letters*, *79*(5), 716–722.
692   https://doi.org/10.1785/gssrl.79.5.716
693   Minson, S. E., Baltay, A. S., Cochran, E. S., Hanks, T. C., Page, M. T., McBride, S. K., Milner, K. R., & Meier, M. A. (2019).
694   The Limits of Earthquake Early Warning Accuracy and Best Alerting Strategy. *Scientific Reports*, *9*(1).
695   https://doi.org/10.1038/s41598-019-39384-y
696   Minson, S. E., Cochran, E. S., Wu, S., & Noda, S. (2021). A Framework for Evaluating Earthquake Early Warning for an
697   Infrastructure Network: An Idealized Case Study of a Northern California Rail System. *Frontiers in Earth Science*, *9*, 450.
698   https://doi.org/10.3389/FEART.2021.620467/BIBTEX
699   Nakamura, Y. (1988). On the urgent earthquake detection and alarm system (UreDAS). *Proc. 9th World Conf. Earthq. Engr.*, *6*,
700   1–6. https://cir.nii.ac.jp/crid/1572261548970160896
701   Nakamura, Y., & Saita, J. (2007). UrEDAS, the earthquake warning system: Today and tomorrow. In *Earthquake Early Warning
702   Systems*. https://doi.org/10.1007/978-3-540-72241-0_13
703   Pacor, F., Paolucci, R., Luzi, L., Sabetta, F., Spinelli, A., Gorini, A., Nicoletti, M., Marcucci, S., Filippi, L., & Dolce, M. (2011).
704   Overview of the Italian strong motion database ITACA 1.0. *Bulletin of Earthquake Engineering*, *9*(6), 1723–1739.
705   https://doi.org/10.1007/s10518-011-9327-6
706   Rados, J., Rados, B., & Kolar, V. (2010). European Train Control System. *Annals of DAAAM and Proceedings of the
707   International DAAAM Symposium*, 277–301. https://doi.org/10.1007/978-3-642-14509-4_7
708   Rovida, A., Locati, M., Camassi, R., Lolli, B., & Gasperini, P. (2020). The Italian earthquake catalogue CPTI15. *Bulletin of
709   Earthquake Engineering*, *18*(7), 2953-2984.
710   Sato, T., & Hirasawa, T. (1973). Body Wave Spectra From Propagating Shear Cracks. *Journal of Physics of the Earth*, *21*(4),
711   415–431. https://doi.org/10.4294/JPE1952.21.415
712   Satriano, C., Wu, Y. M., Zollo, A., & Kanamori, H. (2011). Earthquake early warning: Concepts, methods and physical grounds.
713   *Soil Dynamics and Earthquake Engineering*, *31*(2), 106–118. https://doi.org/10.1016/j.soildyn.2010.07.007
714   Strauss, J. A., & Allen, R. M. (2016). Benefits and Costs of Earthquake Early Warning. *Seismological Research Letters*, *87*(3),
715   765–772. https://doi.org/10.1785/0220150149
716   Stucchi, M., Meletti, C., Montaldo, V., Akinci, A., Faccioli, E., Gasperini, P., Malagnini, L., & Valensise, G. (2004). Pericolosità
717   sismica di riferimento per il territorio nazionale MPS04. In *Istituto Nazionale di Geofisica e Vulcanologia (INGV)*.
718   Tan, M., Hu, Q., Wu, Y., Lin, J., & Fang, X. (2024). Decision-making method for high-speed rail early warning system in
719   complex earthquake situations. *Transportation Safety and Environment*, *6*(3). https://doi.org/10.1093/TSE/TDAD034
720   Yamamoto, S., & Tomori, M. (2013). Earthquake Early Warning System for Railways and its Performance. *Journal of JSCE*,
721   *1*(1), 322–328. https://doi.org/10.2208/JOURNALOFJSCE.1.1_322
722   Yu, H., Ma, Y., & Yu, T. (2023). High-Speed Railway Earthquake Early Warning Testing System Based on LabVIEW.
723   *Advances in Transdisciplinary Engineering*, *34*, 45–54. https://doi.org/10.3233/ATDE230008
724   Zhang, G., Yang, L., & Jiang, W. (2024). Key technologies of earthquake early warning system for China's high-speed railway.
725   *Railway Sciences*, *3*(2), 239–262. https://doi.org/10.1108/RS-11-2023-0046
726   Zhu, J., Sun, W., Li, S., Yao, K., & Song, J. (2024). Threshold-based earthquake early warning for high-speed railways using
727   deep learning. *Reliability Engineering & System Safety*, *250*, 110268. https://doi.org/10.1016/J.RESS.2024.110268
728   Zhu, W., Liu, K., Wang, M., & Koks, E. E. (2020). Seismic Risk Assessment of the Railway Network of China's Mainland.
729   *International Journal of Disaster Risk Science*, *11*(4), 452–465. https://doi.org/10.1007/S13753-020-00292-9/FIGURES/9
730
731
732
733
734
735
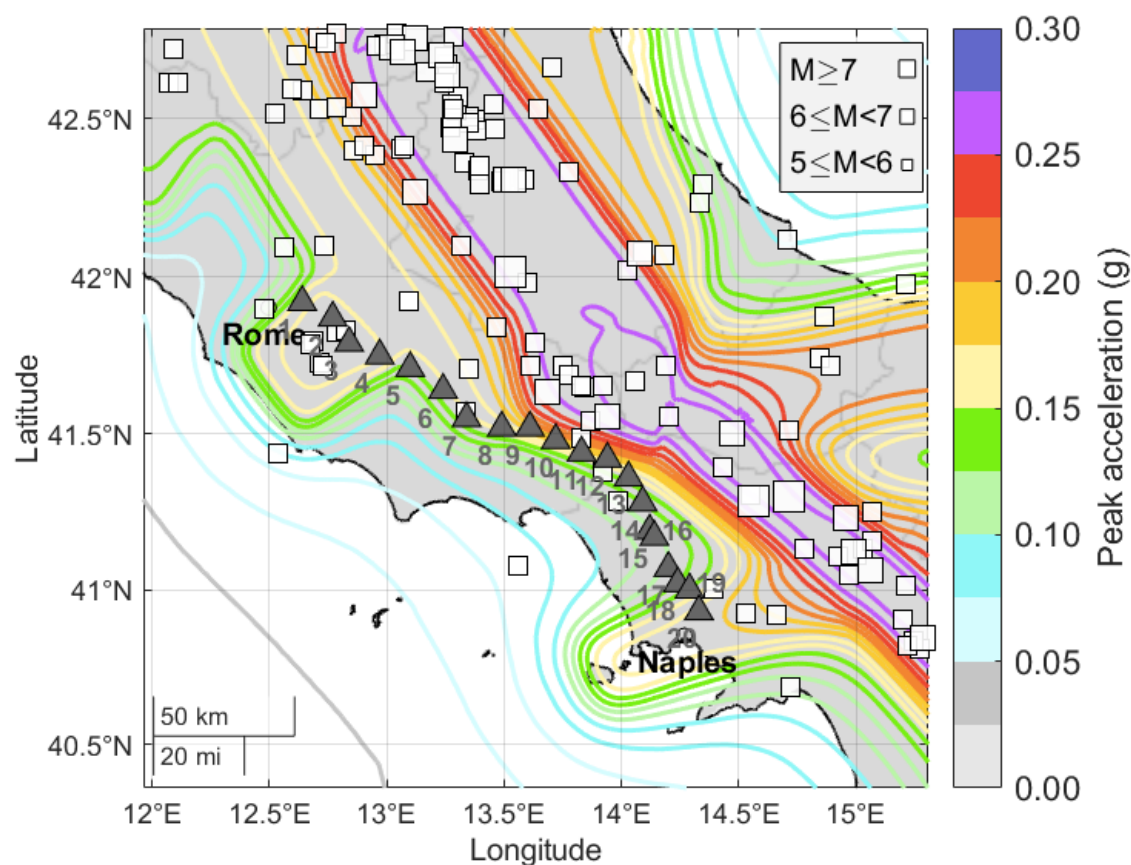
Figure 1. Target area and lines. Map of the seismic network along the RFI high-speed railway for the Earthquake Early Warning application. The 20 stations are represented as dark gray triangles (with an average distance of about 10 km). The background color shows the peak ground acceleration with an exceedance probability of 10% in 50 years according to MPS04 (Stucchi et al., 2004). White squares shows the most relevant events occurred since 1000 according to CPTI15 historic database (Rovida et al., 2020).

a) AlpEW Physical Layout

b) AlpEW Seismic Processing

746

747
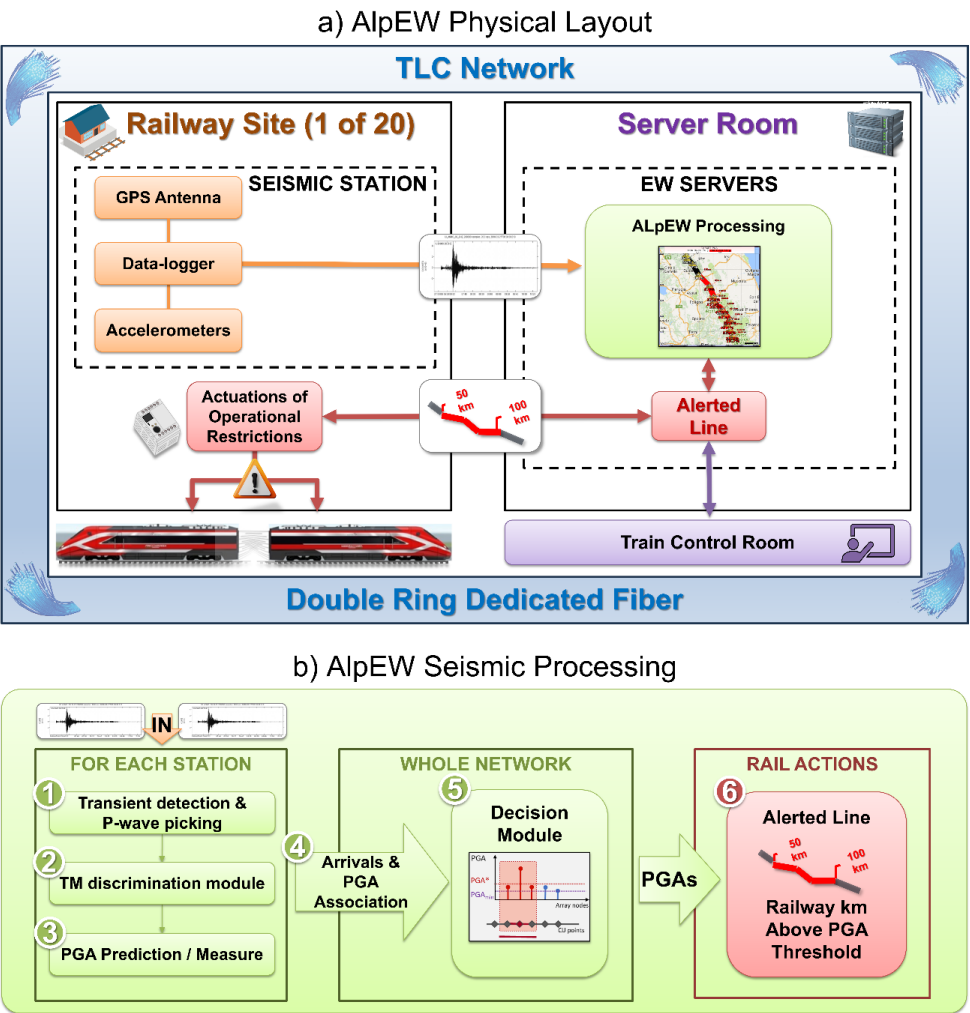
Figure 2. Block diagram of the AlpEW system. a) ALpEW Physical Layout: Left: installed instruments in one of the twenty RFI Technological Sites. The seismic stations record and transmit the continuous data streams containing the 3-component ground motion from all the accelerometers of the RFI network. Right: The AlpEW software installed at the server level. The main output of the seismic processing module is the Alerted Segment of the Railway (ASR) i.e., the evolutive identification of the railway segments above the PGA threshold (kilometric ranges) where operational restrictions are applied. Still at server level, the graphical user interfaces are used for monitoring the state and the Early Warning outputs, and for

755   controlling the train operation. The light blue ring around represents the dedicated fiber optics

756   telecommunication line across the railway, between sites and the server room.

757   b) AlpEW seismic processing: the inputs are the continuous data from the seismic network. Left panel (1 to

758   3) shows the modules implemented at each node: the identification of the arrival times and the

759   corresponding predicted/measured PGAs at each station, after discriminating the potential seismic signals

760   from the train noise. Center panel (4-5) shows the network-level data association. Here, the decision-

761   making module continually analyses the available arrival times and PGAs from all stations and declares an

762   alert when it identifies an earthquake whose impact on the railway is above the threshold. Right panel (6)

763   represents the outcome of the system and the actions on the railway: during the alert, the evolutionary ASR

764   is continually updated and provided as output.

765

766

767

768

769

770

771

772

773

774

775

776

777

778

779
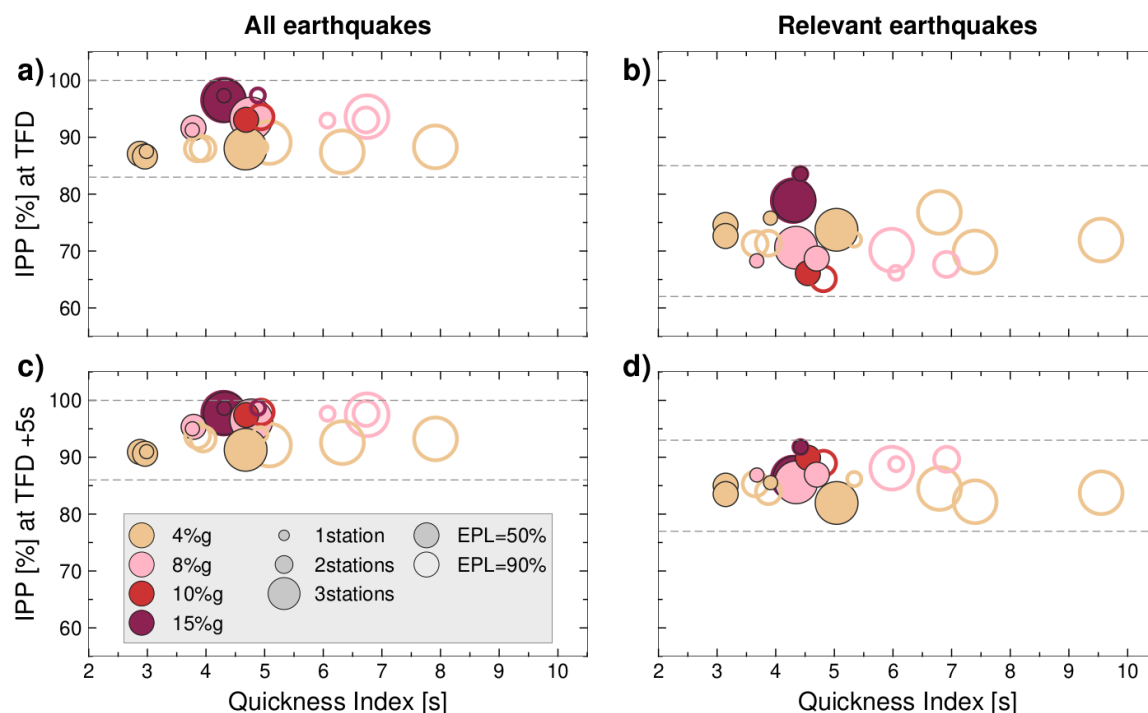
Figure 3. Performance Analysis. The figure shows the IPP parameter as a function of QI at the time of the first declaration (TFD) for all events (a) and for relevant earthquakes only (b) and the IPP vs QI at the time of the first declaration + 5 s for all earthquakes (c) and for relevant earthquakes only (d). In all panels: the size of the symbols increases with the increasing complexity of the Decision Module (i.e., if 1, 2 or 3 stations are used for the first alert release); the color shows the PGA threshold value; filled circles are associated to EPL = 50%; empty circles are associated to EPL = 90%.
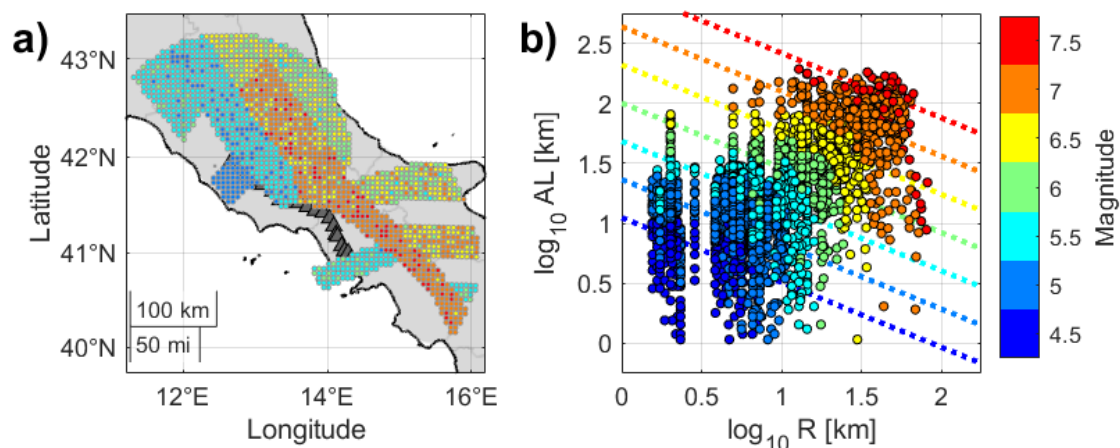
Figure 4. Alerted Segment of the Railway computation. a) Catalogue used for the simulations. Each

point represents co-located earthquakes with a maximum magnitude represented by the color. b) Length of

the ASR as a function of the minimum distance (R) from the railway and of magnitude (color). The dotted

lines represent equation (4) at different magnitude values, and they are colored according to colorbar.
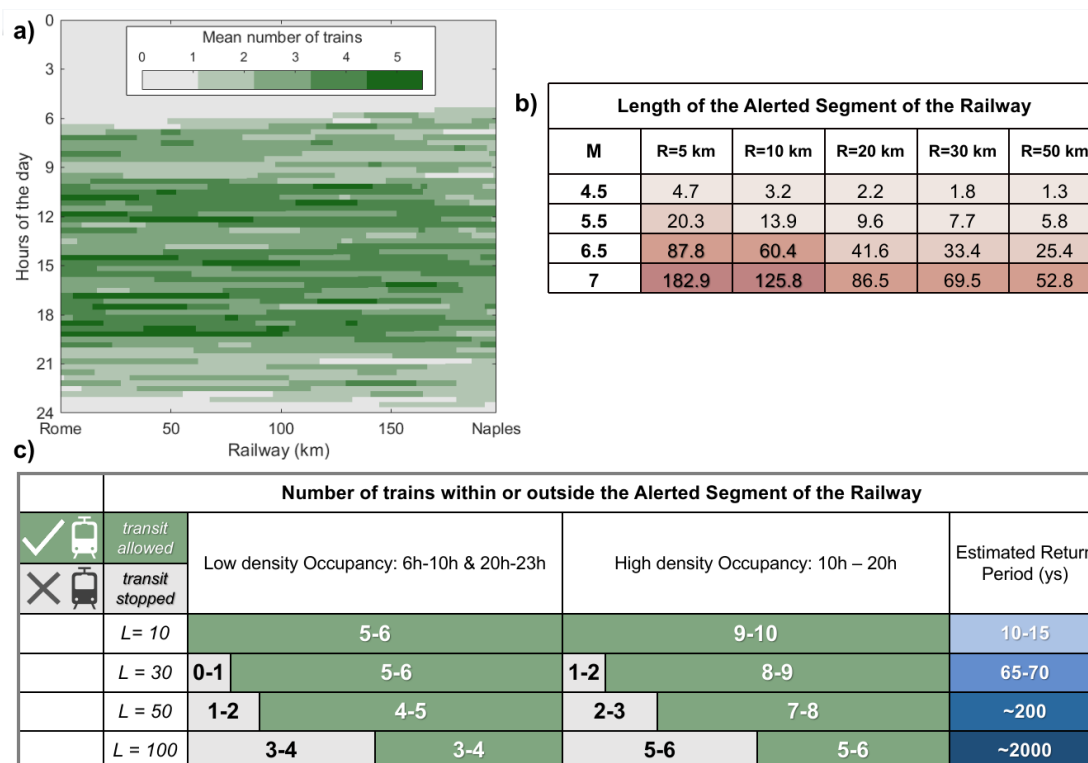
Figure 5. Impact on the railway traffic. a) mean number of trains during different hours of the day, based on a two-month track record of train transit on the RM-NA line. b) length of the Alerted Segment of the Railway (in km), as a function of the magnitude of the event (rows) and distance from the railway line (columns). c) the figure shows the average number of trains travelling within or outside the Alerted Segment of the Railway, for specific values of the segment lengths (rows). The average number of trains is computed for two different time slots of the day, corresponding to a low-density occupancy interval (left columns, 6h-10h & 20h-23h) and to a high-density occupancy interval (10h – 20h). Green segments represent those portions of the line in which the train traffic would be allowed, while gray segments are those in which the traffic would be stopped. The estimated return period for each case is also shown.